

Fluorescent *vic*-dioxime-type ligand and its mono- and dinuclear complexes: The preparation, spectroscopy, and electrochemistry of its various complexes

Metin Özer ^a, Mehmet Kandaz ^{b,*}, Ali Rıza Özkaya ^a, Mustafa Bulut ^{a,*}, Orhan Güney ^c

^a Department of Chemistry, Marmara University, 34722 Kadıköy, Istanbul, Turkey

^b Department of Chemistry, Sakarya University, 54140 Serdivan, Sakarya, Esentepe, Turkey

^c Department of Chemistry, Technical University of Istanbul, 34469 Maslak, Istanbul, Turkey

Received 15 July 2006; received in revised form 17 August 2006; accepted 17 August 2006

Available online 18 October 2006

Abstract

A new coumarin functionalized *vic*-dioxime, *S,S*-bis-[4-methylcoumarinyl]-dithioglyoxime (LH₂), and its soluble mono- and dinuclear complexes {nickel(II), copper(II), cobalt(II), and uranyl(II)} have been reported. The fluorescent properties of the ligand and its complexes are due to the 7-mercapto-4-methylcoumarin fluorophore, which is conjugated with *vic*-dioxime that functions as the MN₄ core. Fluorescence spectra of the probe showed a clear shift in excitation wavelength maxima upon metal binding indicating its potential use as ratio-metric metal indicator. The fluorescence of complexes was found to be highly sensitive to both polarity and protic character of the solvent used. Both mononuclear (LH)₂M (M = Ni, Cu and Co) and homodinuclear (LH)₂(UO₂)₂(OH)₂ complexes have been obtained with the metal:ligand ratios of 1:2 and 2:2, respectively. The characterizations of all newly synthesized compounds were made by elemental analysis, ¹H NMR, FT-IR, UV–vis, and mass (LSI–MS) data. The electrochemical investigation of the Ni(II), Cu(II), Co(II) and UO₂(II) complexes in comparison with the ligand involving oxime and coumarin moieties enabled us to identify metal-, oxime- and coumarin-based signals.

© 2006 Elsevier Ltd. All rights reserved.

Keywords: *Vic*-dioxime complexes; Coumarin; Fluorescence; Nickel; Copper; Cobalt; Uranyl; Cyclic voltammetry

1. Introduction

Recent investigations on both *vic*-dioximes and coumarins have stimulated considerable interest not only in academic investigations, but also in industry due to potentially wide applications [1–4]. Coumarin derivatives or compounds based on the coumarin ring system have been some of the most extensively investigated and commercially significant group of organic fluorescent materials in recent years. Many products that contain the coumarin subunit exhibit useful and diverse biological activity and find their application in

pharmaceuticals, fragrances, agrochemicals, insecticides and polymer science. They also play a vital role in electrophotographic, electroluminescent devices and laser dyes [3–6]. These properties have made coumarins into interesting targets for organic and inorganic chemists. An attachment of coumarin on the *vic*-dioxime would produce various different signals on UV–vis, fluorescent, NMR, and mass spectra. There remains great interest in the molecular design and synthesis of new coumarin derivatives which would extend the available range of long wavelength emitting fluorescent materials. So far, great effort has been made in the incorporation of functional groups on the periphery of the *vic*-dioxime molecule to modify its conformational, optical and redox properties [7–9]. Although a large number of *vic*-dioxime complexes

* Corresponding authors. Fax: +90 264 295 59 50 (M.K.).

E-mail address: mkandaz@sakarya.edu.tr (M. Kandaz).

with peripheral donor types such as, MS_2 , MN_4 , MN_2S_2 , MS_4 , $MN_2S_2O_2$, and MO_4S_2 have been synthesized and characterized [8–15], transition metal *vic*-dioxime complexes with peripheral functional fluorescent coumarin substituents have not been studied in coordination chemistry to the best of our knowledge.

Compounds derived from the basic coumarin structural unit are also widely used as laser dyes. As most of the coumarins provide blue–green colours, there is a huge interest in the design of new derivatives emitting in the yellow–red region of the visible spectrum. To achieve this purpose, it is essential to isolate and correctly describe the excited state(s) of the molecular structures involved in the fluorescence process. Oxidation states of the central metals, type and number of donor atoms and core structures of the complexes are major factors to determine structure–function relationships of the transition metal complexes. The stability of the oxidation states of the metal center in these complexes depends on the metal coordination environment [16,17]. The ability of donor atoms to stabilize reduced and/or oxidized forms of metal has sparked interest in their role in bioinorganic systems. Hence, for a better understanding of their properties, the investigation of redox behaviour has a vital importance. Although various oximes and their metal and non-metal compounds have been studied extensively, electrochemistry of *vic*-dioximes is scarce [8,12,14].

So, in this study, we report on the synthesis and characterization of a ligand containing both coumarin and *vic*-dioxime, and its transition metal complexes as multi-addressable compounds and present a new fluorescent chemosensor for some transition metals, which was obtained by conjugating 7-mercapto-4-methylcoumarin fluorophore and *vic*-dioxime as metal-chelating moiety. The redox properties of the metal complexes synthesized in this study were investigated by cyclic and differential pulse voltammetry, as compared with the ligand involving oxime and coumarin moieties.

2. Experimental

2.1. Synthesis

(*E,E*)-dichloroglyoxime was prepared by a reported procedure [18,19]. 7-Mercapto-4-methylcoumarin was obtained from Fluka Chemical Co. All reagents and solvents were of reagent-grade quality, obtained from commercial suppliers and used without further purification. Mass spectra were recorded on a Varian 711 and VG Zapspec spectrometer. FT-IR spectra were recorded on a Mattison 1000 FT-IR spectrometer and electronic spectra on a Unicam UV-2401 p.c. spectrophotometer. 1H NMR spectra were recorded on a Bruker 250 MHz spectrometer. Elemental analysis (C, H, and N) was performed at the Instrumental Analysis Laboratory of Marmara University. Metal contents were determined with a Hitachi 180-80 Atomic Absorption Spectrometer in solution prepared by decomposition of the compounds in aqua regia followed by dilution with water.

2.2. *S,S*-bis-[4-methylcoumarinyl]-dithioglyoxime (LH_2) (**1**)

To 50 cm³ of a solution of 7-mercapto-4-methylcoumarin (2.44 g, 12.73 mmol) and 1.3 g of anhydrous NaHCO₃ (excess) in absolute MeOH which was stirred at room temperature for 0.5 h under N₂ atmosphere, 20 cm³ solution of 1.0 g (*E,E*)-dichloroglyoxime (6.36 mmol) in dry MeOH was added dropwise during 0.5 h. The mixture was stirred at room temperature for 2 h. The colour of the solution was turned into light yellow during the time and the reaction mixture was kept at reflux temperature for an additional 4 h with stirring. The reaction mixture was allowed to cool at room temperature. After filtration of sodium chloride formed, the volume of the reaction mixture was reduced to dryness. The excess of 7-mercapto-4-methylcoumarin and (*E,E*)-dichloroglyoxime starting material was removed by washing the solution with first water, alcohol and acetone. The creamy powder was dried *in vacuo* at room temperature. This compound is soluble in DMF, DMSO, pyridine and quinoline and insoluble in MeOH, EtOH, and THF.

Yield: 1.40 g (47%); m.p.: 260 °C, ν_{max} (cm⁻¹, thin film): 3209.3 (N–OH), 2970.2 (Aliph-H), 1706.9 (H-Bond), 1688 (C=C), 1602 (C=N), 1540.1, 1387–1302 (Ar-skel. vib.), 1179.4, 998.1, 960.5 (N–O), 826.4, 778.2, 574.7, 518.8. 1H NMR (DMSO-*d*₆, 300 MHz) δ : 12.63 (s, 2H, =N–OH, D₂O-exchangeable), 7.65 (dd, 2H, Ar–H), 7.32 (dd, 2H, Ar–H, *ortho* to CH₃Ar), 7.05 (s, 2H, Ar–H, *ortho* to Ar–S–), 6.40 (dd, Ar–H, 2H, *ortho* to –COO), 2.42 (s, 6 H, –CH₃). ^{13}C NMR (300 MHz, δ , DMSO-*d*₆): 162.20 (C=O), 154.58 (C=N), 153.11 (C–O), 143.25 (C–H, *meta* to C=O), 136.37 (C–CH₃), 134.77 (C–S), 126.21 (C–C–CH₃), 120.92 (C–CS), 117.26 (C–CS), 115.46 (C–C=O), 40.23 (DMSO), 18.76 (CH₃) ppm. UV–vis (in DMF) λ_{max} (nm) (log ϵ): 333 (12.10), 403 (sh, 3.20). Laser Spray Ionization Mass Spectrometer (LSI–MS, Scan ES⁺): *m/z* (%): 470.53 (5) [M + 2]⁺, 356.21 (40), 272.24 (8) [M], 250.27 (10) [M – OH]⁺, 242.20 (5) [M – NOH]⁺, 209.16 (5) [M – 4 × OH]⁺, 195.08 (10), 181.13 (15) [M – C₃H₄O₂S], 172.12 (17).

2.3. *N,N'*-coordinated mononuclear complexes, [M(HL)₂], M = Ni(II), Cu(II), Co(II) (**2**, **3** and **4**)

To a solution of **1** (0.15 g, 0.32 mmol) in DMF (ca. 30 cm³) was added dropwise with stirring a THF solution of about 10 cm³ of the appropriate metal salt; [Ni(NO₃)₂·6H₂O] (0.046 g, 0.16 mmol); Cu(NO₃)₂·6H₂O (0.047 g, 0.16 mmol), Co(NO₃)₂·6H₂O (0.046 g, 0.16 mmol) at room temperature for 1–2 h. A distinct change in colour and a decrease in the pH value of the solution were observed. The resulting mixture was then additionally stirred at about 50 °C for 3 h to complete the reaction. An equivalent amount of (C₂H₅)₃N in THF was added dropwise to maintain a pH value at about 6.5–7.0 and an extra precipitation was completed leading to (*E,E*)-Ni(LH)₂, (*E,E*)-Cu(LH)₂, and (*E,E*)-Co(LH)₂. All the mononuclear complexes were separated as powders. Then the mixture was firstly filtered, washed

successively with water, alcohol, THF, acetone and Et₂O to remove unreacted organic and inorganic impurities. The moisture sensitive products dried in a vacuum desiccator over CaCl₂. These compounds are soluble in DMF, DMSO, pyridine, and quinoline and insoluble in MeOH, EtOH, CHCl₃, CH₂Cl₂ and THF.

2.3.1. (E,E)-Ni(LH)₂ (2)

Yield: 0.044 g (27.72%); m.p.: >200 °C. ν_{\max} (cm⁻¹): 3417 (N–OH), 3244 (N–OH), 3080 (w, Ar–H), 2985, 2930 (w, Aliph–H), 1716 (m, O–H···O bridge), 1718 (w, O–H···O bridge), 1654 (C=C), 1596 (C=N), 1544, 1404, 1257, 1174, 1056, 962 (s, N–O) 858, 833, 773, 750, 709, 667 (S–CH₂) 576. ¹H NMR (DMSO-*d*₆, 300 MHz, δ): 16.48 (s, 2H, O···H···O, D₂O-exchangeable), 7.95 (dd, 2H, Ar–H), 7.78 (s, 2H, Ar–H, *ortho* to CH₃Ar), 7.20 (dd, 2H, Ar–H, *ortho* to Ar–S–), 6.24 (s, Ar–H, 2H, *ortho* to –COO), 2.44 (s, 6H, –CH₃). UV–vis (in DMF) λ_{\max} (nm) (log ϵ): 552 (0.20), 456 (sh, 0.25), 336 (0.95), 292 (0.85, sh), 267 (sh, 0.80). MS (LSI, Scan ES⁺): *m/z* (%): 1017.13 (5) [(M+Na)]⁺, 993.27 [(M)]⁺, 948.41, 846.63, 835.54, 803.19, 710.22, 507.18, 489.06, 421.47, 422.95, 423.38 (100), 317.24, 270.18, 258.27, 205.13, 167.06.

2.3.2. (E,E)-Cu(LH)₂ (3)

Yield: 0.047 g (29.44%); m.p.: >200 °C. ν_{\max} (cm⁻¹): 3425 (N–OH), 3066 (Ar–H, w), 2977, 2917 (w, Aliph–H), 1718 (m, O–H···O bridge), 1598 (C=C), 1560 (C=N), 1461, 1382, 1317, 1245, 1172, 1149, 1124, 1056, 1008 (N–O), 949, 858, 833, 769, 752, 705, 663 (S–CH₂), 578. UV–vis (DMF) λ_{\max} (nm): 460 (sh, 0.74), 333 (1.18), 290 (sh, 0.77), 266 (sh, 0.68). MS (LSI, Scan ES⁺): *m/z* (%): 997.15 (10) [(M)]⁺, 490.37 (5), 401.05, 350.01, 312.13, 259.02 (100), 221.07.

2.3.3. (E,E)-Co(LH)₂ (4)

Yield: 0.055 g (34.61%); m.p.: >200 °C. ν_{\max} (cm⁻¹): 3438 (N–OH), 3280, 3074, 2989, 2930 (Aliph–H), 1720 (O–H···O bridge), 1689 (w), 1600 (C=C), 1544 (C=N), 1448, 1388 (st), 1321, 1249, 1174 (st), 1058, 1012 (N–O), 952 (st), 894, 862, 817, 773, 752, 707, 572 (S–CH₂), 544. UV–vis (DMF) λ_{\max} (nm) (log ϵ): 428 (0.21, sh), 335 (1.14), 294 (sh, 0.87), 267 (0.73). MS (LSI, Scan ES⁺): *m/z* (%): 993.80 (5) [(M)]⁺, 290.30 (7), 197.04, 158.14, 130.07.

2.4. Dinuclear U^{VI}O₂ complex [(LH)₂(UO₂)₂(OH)₂] (5)

To a solution of 0.2 g of **1** (0.43 mmol) in DMF (40 cm³), a solution of 0.22 g of UO₂(NO₃)₂(OH)₂ (0.43 mmol) in 10 cm³ THF was added. The colour of the solution turned to orange, and the pH of the mixture immediately dropped to about 5. The mixture was heated on water-bath for ca. 2 h and then at 50–60 °C for 2 h. After adding an equivalent of Et₃N to the mixture with stirring to adjust the pH of the solution to ca. 6.5–7.0, an orange precipitate was produced. The mixture was cooled to room temperature, filtered, and the residue washed with hot water, EtOH, acetone and Et₂O, and finally dried *in vacuo*. These compounds are soluble in DMF,

DMSO, pyridine, and quinoline and insoluble in MeOH, EtOH, CHCl₃, CH₂Cl₂ and THF.

Yield: 0.062 g (11.83%); m.p.: >200 °C. ν_{\max} (cm⁻¹): 3429 (N–OH), 3244 (sh), 3083, 2991, 2943 (Aliph–H), 1718 (w), 1604 (C=C), 1548 (st, C=N), 1487, 1396, 1137 (N–O), 917 (st, O=U=O), 813, 684, 460. ¹H NMR (DMSO-*d*₆, 300 MHz) δ : 12.78 and 12.46 (s, 2H, N–OH D₂O-exchangeable), 7.66 (dd, 2H, Ar–H), 7.34 (dd, 2H, Ar–H, *ortho* to CH₃Ar), 6.98 (s, 2H, Ar–H, *ortho* to Ar–S–), 6.37 (dd, Ar–H, 2H, *ortho* to –COO), 2.44 (s, 6H, –CH₃). UV–vis (in DMF) λ_{\max} (nm) (log ϵ): 437 (sh, 0.02), 342 (sh, 0.17), 257 (0.51). MS (LSI, Scan ES⁺): *m/z* (%): 1509.1 [(M)]⁺, 1218.5, 578.0, 499.4, 472.2, 319.2, 235.0 (100), 192.0, 156.2, 130.0, 123.0.

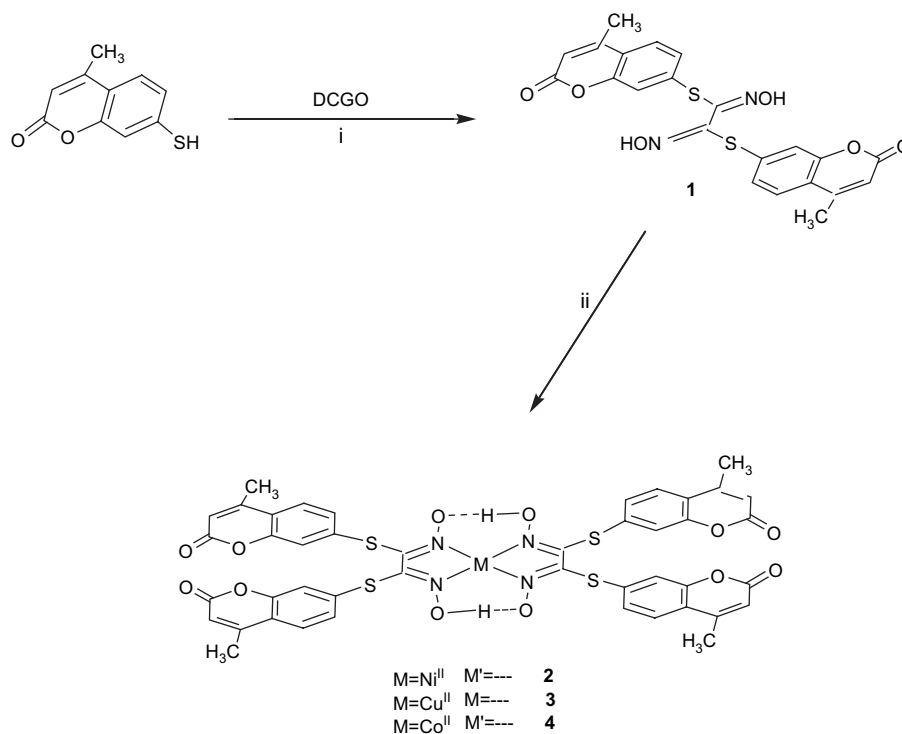
2.5. Electrochemistry

Tetrabutylammonium perchlorate (TBAP) (Electrochemical grade, Fluka Chemical Co) as the supporting electrolyte and extra pure dimethylsulfoxide (DMSO) (Fluka Chemical Co) as the solvent were used in electrochemical measurements. Electrochemical measurements were carried out with a Princeton Applied Research Model VersaStat II potentiostat/galvanostat, controlled by an external PC, utilizing a three-electrode configuration at 25 °C. A saturated calomel electrode (SCE) was employed as the reference electrode. A platinum spiral wire was used as the auxiliary electrode. The working electrode was a platinum with an area of 0.12 cm² in the measurements. The surface of the platinum working electrode was polished with an H₂O suspension of Al₂O₃ before each run. The last polishing was done with a particle size of 50 nm. The ferrocene/ferrocenium couple (Fc/Fc⁺) was used as an internal standard. Solutions were deoxygenated by a stream of high-purity nitrogen for at least 15 min prior to running the experiment, and the solution was protected from air by a blanket of nitrogen during the experiment. For the controlled-potential coulometry (CPC) studies, a platinum gauze working electrode, a platinum wire counter electrode separated with a bridge, an SCE as reference electrode, and a model 377/12 synchronous stirrer were used.

3. Results and discussion

3.1. Material and equipments

S,S-bis-[4-methylcoumarinyl]-dithioglyoxime (LH₂) (**1**) was prepared by the reaction between 7-mercapto-4-methylcoumarin and (E,E)-dichloroglyoxime in the presence of Na₂CO₃ base (Scheme 1). A new pale white powder *vic*-dioxime was isolated in a considerably moderate yield. This compound is soluble in limited common organic solvents, such as DMF, DMSO, quinoline, pyridine, DMAA and insoluble in MeOH, EtOH, CHCl₃, MeCN and THF. The polar coumarin moieties do not increase the solubility of **1** (LH₂) enough in organic polar solvents. Coumarin attached mononuclear complexes [(LH)₂M] [M = Ni(II) (**2**), Cu(II) (**3**), Co(II) (**4**)] (Scheme 1) and dinuclear complex [(LH)₂(UO₂)₂(OH)₂] (**5**) (Fig. 1) were achieved at room



Scheme 1. (i) MeOH, DCGO, Reflux, NaHCO₃, (ii) MX₂·6H₂O (M = Ni^{II}, Cu^{II}, Co^{II}, UO₂²⁺). X = NO₃²⁻; Et₃N, THF.

temperature, using a metal/ligand molar ratio 1:2 for the mononuclear and 2:2 for the dinuclear substituted *vic*-dioxime complexes. These products were isolated as analytically pure species via spontaneous precipitation. Further precipitation was achieved by adding triethylamine to the crude product after the first precipitation [20–25].

The structural formula of **1** and its complexes were deduced by elemental analysis, spectroscopic and mass spectral data. The colours, yields and elemental analyses of (**1**) and its complexes are listed in Table 1. In the IR spectrum of **1**, the $\nu(-NOH)$, $\nu(C=N)$ and $\nu(N-O)$ characteristic stretching vibrations are observed at 3232, 1588, and 984 cm⁻¹, respectively. However, the weak (O–H···O) deformations are observed at 1700–1750 cm⁻¹ as a broad weak absorption, and the stretching absorptions of the N–OH have disappeared upon addition of deuterium oxide (D₂O) in mononuclear **2–4** compounds, which also confirm the formation of mononuclear structure [2,8–15,22–25]. On the other hand, the strong bands at around 917, 1137, and 3244 cm⁻¹ in IR spectrum of [(LH)₂(UO₂)₂(OH)₂] complex were characterized for $\nu(O=U=O)$, $\nu(N-O)$, and $\nu(N-OH)$ vibrations as broad bands. The ¹H NMR data gave reasonable information about the proposed structure of *vic*-dioxime ligand (**1**) together with ¹³C NMR and its nickel and uranyl complexes. A singlet at $\delta = 12.63$ (s, 2H, =N–OH, D₂O-exchangeable) in the ¹H NMR spectrum of **1** in DMSO-*d*₆ is assigned to =N–OH. Four different H atoms together with the nine different C atoms on the coumarin moieties were easily determined with ¹H and ¹³C NMR. The ¹H NMR spectra of the diamagnetic complex **2** was characterized by the disappearance of the

N–OH signal which appeared at 12.63 ppm in **1**, and the existence of intramolecular deuterium-exchangeable H-bridge protons was observed by a new signal at lower field, $\delta = 16.48$ ppm. Consequently, we may conclude that both of these *d*⁸ metal ions are coordinated with the dioximate donor sites in square planar geometry [2,8–15,20,22–25]. The ¹H NMR signal for the coumarin moieties were similar to what was observed for **1** except for a slight shift. As expected, the (*E,Z*)-[(LH)₂(UO₂)₂(OH)₂] (**5**) complex has a tetrahedral and paramagnetic structure and its NMR signals are broad. The NMR spectrum of **5** contains two peaks for N–OH corresponding to oxime group in low field ($\delta = 12.78, 12.46$ ppm, s, 2H, N–OH, D-exchangeable), which can be attributed to the magnetic anisotropy of the uranyl ion as discussed previously in reports of the Bekaroglu group and our works [8–15,20,26]. It is known that uranyl ions enhance the chemical shift differences between the non-equivalent protons. The UV–vis spectra of the ligand and its complexes (**2–5**) in

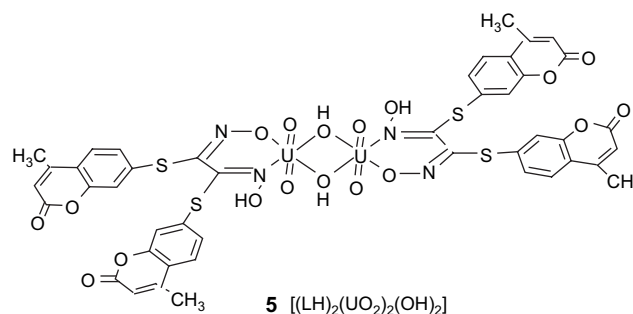


Fig. 1. Binuclear uranyl complex (**5**).

Table 1
Analytical and physical data for LH₂ and its complexes

Compounds	Colour	Calc. (found) (%)			
		C	H	N	M'
(1) LH ₂	Creamy	56.41 (56.12)	3.42 (3.30)	5.98 (5.87)	–
(2) (E,E)-Ni(LH) ₂	Reddish-brown	53.22 (52.87)	3.04 (3.01)	5.63 (5.55)	5.84 (5.80)
(3) (E,E)-Cu(LH) ₂	Brown	52.93 (52.22)	3.03 (3.00)	5.62 (5.37)	6.36 (6.28)
(4) (E,E)-Co(LH) ₂	Dark-brown	53.17 (52.85)	3.04 (2.98)	5.64 (5.47)	5.94 (5.91)
(5) (LH) ₂ (UO ₂) ₂ (OH) ₂	Orange	35.03 (34.73)	2.14 (2.20)	3.71 (3.65)	–

DMF showed two or three absorption bands between 260 nm and 450 nm. These bands are assigned to both charge transfer transition from the metal to the π^* anti-bonding orbital of ligand and spin-allowed $\pi-\pi^*$ transition of the C=N group of the oxime ligand which is seen at about 300 nm [20,22–26].

The results of elemental analysis, LSI–MS and AAS confirmed mono- and dinuclear complexation with Ni²⁺, Cu²⁺ and Co²⁺. The metal contents of the trinuclear complexes were also determined quantitatively by atomic absorption spectrophotometry.

3.2. Absorption spectra

To understand the effects of different transition metal ions on the optical properties of LH₂, **1**, we measured the absorption spectra of **1** and its mononuclear complexes. Fig. 2 gives the UV–vis spectra of oxime ligand and its complexes in DMF. It can be seen from Fig. 2 that absorption maxima of the oxime ligand shift to red upon metal ions binding. Absorption maximum wavelength of compound **1** shifts 1 nm for **3**, 9 nm for **2** and 13 nm for **4** complexes. This red shift can be explained by the reduction of the HOMO–LUMO band gap [4,27]. When oxime ligand is bound to metal ion, HOMO–

LUMO band gap reduces compared with that free oxime, resulting in the red shift of absorption spectra.

3.3. Fluorescence measurements

As seen from Fig. 3 (above), **1** (LH₂) exhibits an excitation maximum wavelength at 340 nm, which shifts to 336 nm upon binding to transition metal ions. Meanwhile, decrease in excitation intensity of oxime ligand is observed depending on complex formation with transition metal ions. When excited at 340 nm, LH₂ shows an emission maximum at 400 nm, which does not shift upon binding of transition metal ions (Fig. 3 (bottom)). From this figure, it is evident that fluorescence emission intensity of **1** decreases dramatically depending on complex formation with transition metal ions. This decrease of emission intensities is due to the formation of coordination complex of N-atom on compound **1** with metal ions. These coordination complexes make the energy transfer from the excited state of *vic*-dioxime ligand to metal ions possible, thus increase the non-radiated transition of *vic*-dioxime ligand excited state and decrease the fluorescence emission. On the other hand, degree of fluorescence quenching increases upon complex formation with metal ion which has lower d-orbital electron number. Decrease in emission maxima was in the order of Cu²⁺ < Ni²⁺ < Co²⁺ for the complexes synthesized (Fig. 3).

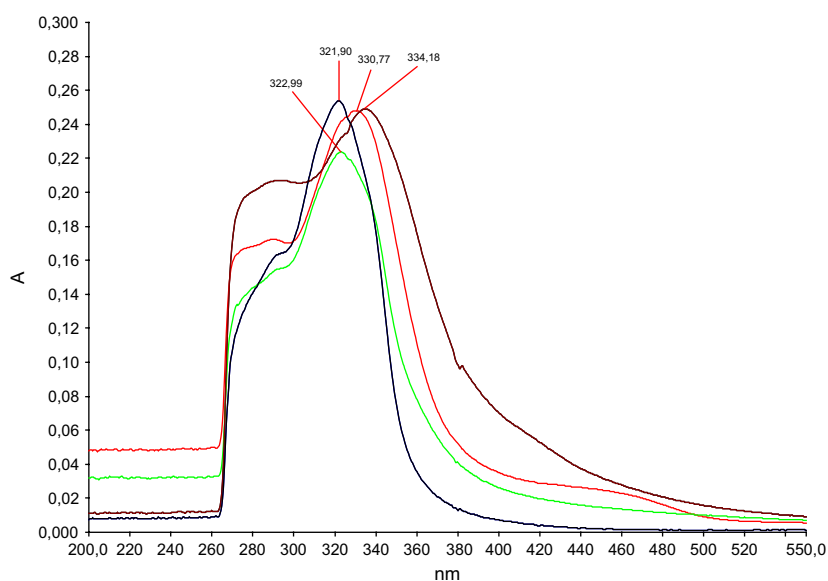


Fig. 2. Absorption spectra of oxime ligand (**1**) and its complexes (**2**, **3**, **4** and **5**) in DMF.

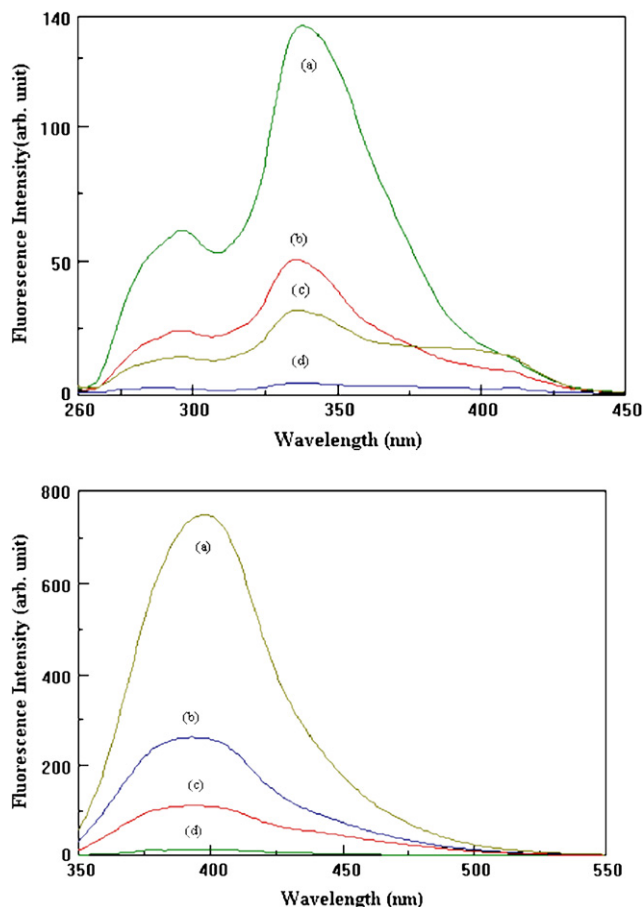


Fig. 3. Excitation (above) and emission (bottom) spectra of 10^{-5} M LH₂ (a) and its complexes with Cu²⁺ (b), Ni²⁺ (c) and Co²⁺ (d) ions in DMF. Excitation and emission slit widths were set at 5 nm.

3.4. Electrochemical measurements

The electrochemical properties of **1–5** were investigated using voltammetric techniques in DMSO/TBAP on platinum working electrode. The results are summarized in Table 2. With the controlled-potential coulometry studies, complete electrolysis of the solution at the working electrode at constant potential (E_{pc} of redox couple) was achieved, and the time integration of the electrolysis current was recorded and the charge, Q , at the end of electrolysis was calculated using the current–time response of solution. Faraday's law was used to estimate the number of electrons transferred. The number of electrons was found to be two for the first reduction processes of **2** and **5** and one for all other redox processes.

First, we carried out the voltammetric measurements of **1** in order to compare its redox behaviour with those of the metal complexes **3–5**, and thus to assign the redox processes of **2–5**. Fig. 4 indicates the cyclic voltammogram (CV) of **1**. CV of **1** displays two one-electron reductions and a one-electron oxidation process (Table 2). The comparison of the redox data of oxime–coumarin ligand **1** with those of our previously reported oxime–metal complexes [9,28] imply that the first oxidation and the first reduction processes probably correspond to the oxime moieties while the second reduction

Table 2
Voltammetric data for **1–5** in DMSO/TBAP^a

Compounds	Redox couple	$E_{1/2}$ or E_p (V) ^b	ΔE_p (V) ^c
1	Ox/Ox ⁺ (I)	0.81	–
	Ox/Ox [–] (IV)	–1.57	–
	Coum/Coum [–] (V)	–1.63	0.18
2	Ox/Ox ⁺ (I)	0.76	–
	Ni(II)/Ni(III) (II)	0.52	–
	Ni(II)/Ni(I) (III)	–0.72	0.24
	Ox/Ox [–] (IV)	–1.22	–
3	Cu(II)/Cu(III) (II)	0.17	0.05
	Cu(II)/Cu(0) (III)	–0.08	0.03
	Ox/Ox [–] (IV)	–1.16	–
	Coum/Coum [–] (V)	–1.59	0.14
4	Co(II)/Co(III) (II)	0.62	0.06
	Co(II)/Co(I) (III)	–0.81	0.14
	Ox/Ox [–] (IV)	–1.35	0.34
	Coum/Coum [–] (V)	–1.46	0.05
5	Ox/Ox ⁺ (I)	0.56	0.10
	U(VI)O ₂ /U(V)O ₂ (III)	–0.73	0.18

^a Half-wave ($E_{1/2}$) or peak (E_p) potentials in DMSO/TBAP versus Fc/Fc⁺ couple correspond approximately with the above data – 0.50 V. These data were measured by cyclic or differential pulse voltammetry.

^b $E_{1/2} = (E_{pa} + E_{pc})/2$ for reversible or quasi-reversible processes. E_p indicates the cathodic peak potential for irreversible reduction processes and the anodic peak potential for irreversible oxidation processes.

^c The peak separation ($\Delta E_p = E_{pa} - E_{pc}$) values are reported at 0.100 V s^{–1}.

process belongs to the coumarin moieties. The oxime-based processes are irreversible while coumarin-based second reduction process has a quasi-reversible character with a peak separation of 0.18 V. Although the first oxidation process (couple I) was recorded as an ill-defined signal during the CV measurement, it was well detected by differential pulse voltammetry (inset in Fig. 4).

Fig. 5 indicates the cyclic voltammograms of **3** at different scan rates on platinum working electrode in DMSO/TBAP.

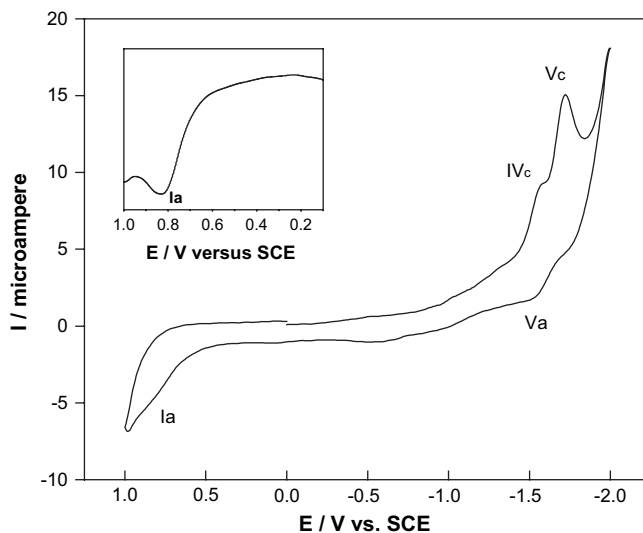


Fig. 4. Cyclic voltammogram of **1** at 0.100 V s^{–1} on Pt in DMSO/TBAP. The inset indicates differential pulse voltammogram at the positive potential side.

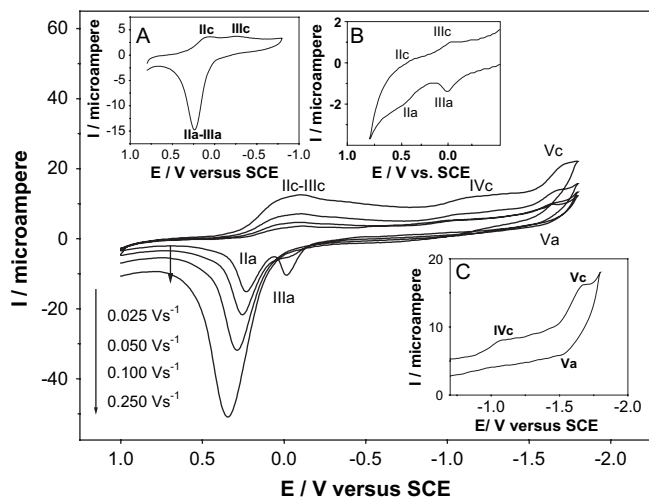


Fig. 5. Cyclic voltammograms of **3** at various scan rates on Pt in DMSO/TBAP. Scan rate: 0.100 V s^{-1} , scan range: $(+0.8)$ – (-0.8) V for inset A. Inset B indicates cyclic voltammogram of **3** at 0.100 V s^{-1} on GCE in DMSO/TBAP. Scan rate: 0.100 V s^{-1} , scan range: (-0.7) – (-1.8) V for inset C.

Complex **3** displays three reduction and an oxidation processes (Table 2). The first reduction (couple III) is a reversible two-electron process with a peak separation of 0.030 V , and may be assigned to Cu(II)/Cu(0) process. On the other hand, the one-electron first oxidation couple (couple II) probably belongs to Cu(II)/Cu(III) process. The anodic peaks of couples II and III are separate at low scan rates, but overlap at high scan rates (Fig. 5 and inset A in Fig. 5). It appears that Cu(I) is unstable towards conversion to Cu(0) which tends to plate out on the electrode surface, as also reported in an article reported previously [29]. Thus, Cu(0) deposited on the platinum electrode during the cathodic scan through the negative potentials is first oxidized to Cu(II) and then to Cu(III) during the reverse scan. The first oxidation process of **3** (IIa in Fig. 5) showed an adsorption behaviour. Direct proportionality of the anodic peak current with scan rate provided an evidence for the adsorption character of this process. This adsorption

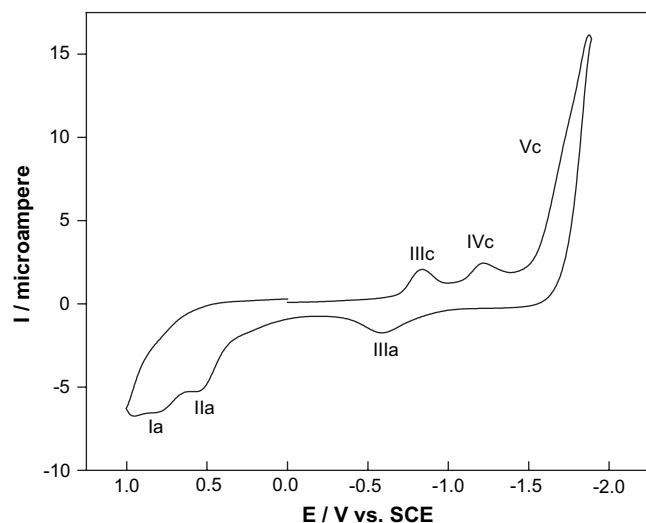


Fig. 6. Cyclic voltammogram of **2** at 0.100 V s^{-1} on Pt in DMSO/TBAP.

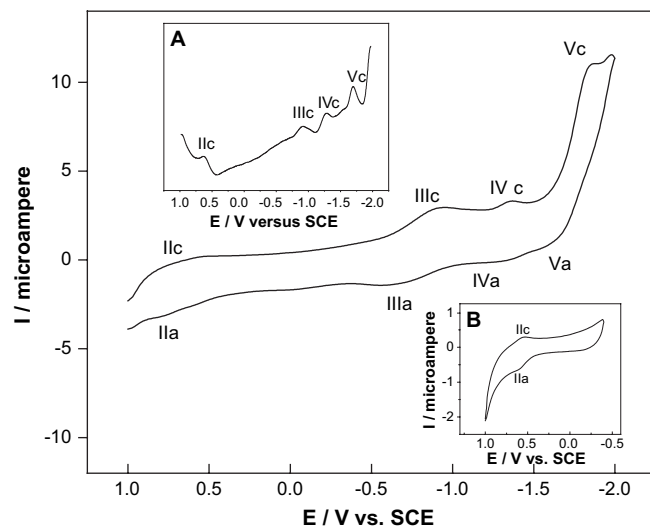


Fig. 7. Cyclic voltammograms of **4** at 0.100 V s^{-1} on Pt in DMSO/TBAP. Inset A shows differential pulse voltammogram of **4**. Scan rate: 0.100 V s^{-1} , scan range: (-0.4) – $(+1.0)$ V for inset B.

behaviour should be due to Cu(0) deposited on the platinum working electrode. We should note that the adsorption behaviour was not observed when the platinum working electrode was replaced with the glassy carbon working electrode. In addition, couples II and III were well-separated at all scan rates studied, as shown for 0.100 V s^{-1} in inset B in Fig. 5. In the case of glassy carbon electrode, it appears that Cu(I) species are stable, and thus the first reduction (couple III) corresponds to Cu(II)/Cu(I) process. Diffusion-controlled nature of the first oxidation process of **3** [Cu(II)/Cu(III) , couple II], i.e., direct proportionality of the peak currents with the square root of scan rate provided an evidence for the assignment of these processes. The comparison of the voltammetric data of **3** with that of **1** suggests that the second and the third reductions (IV and V) are oxime- and coumarin-based processes, respectively (Fig. 5 and inset C in Fig. 5). These ligand-based reduction processes, especially the oxime-based reduction process of **3**

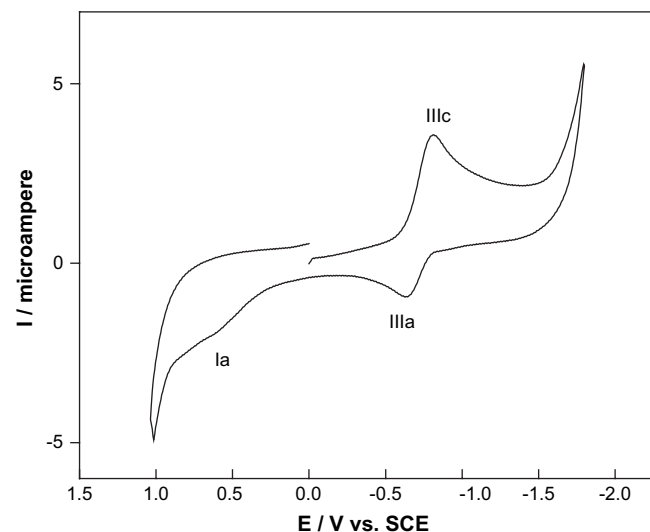


Fig. 8. Cyclic voltammogram of **5** at 0.100 V s^{-1} on Pt in DMSO/TBAP.

(couple IV) occur at the potentials less negative than those of **1**. This behaviour was also observed with complexes **2** and **4**, presumably due to negative charge transfer from ligand to metal during the formation of metal complexes.

The redox chemistry of Ni(II) (**2**) and Co(II) (**4**) complexes exhibited both M(II)/M(III) and M(II)/M(I) redox couples. Figs. 6 and 7 indicate the cyclic voltammograms of **2** and **4**, respectively. First reduction and first oxidation processes for these complexes (couples II and III in Figs. 6 and 7) take place on the metal center of the complexes whose voltammetric data are given in Table 2. It is clearly stated in the literature that oxime containing metal complexes give redox signals involving both higher and lower oxidation states of the metal depending on the coordination environment of metal center [9,28–30]. For both **2** and **4**, the second reduction process (couple IV) corresponds to the oxime moieties. Complex **2** also showed an other one-electron irreversible process (I) which can be assigned to the oxidation of oxime moieties while coumarin-based redox process was not observed. The third reduction process of **4** (couple V) can be assigned to coumarin moieties. As observed for **3**, the ligand-based reduction processes of **2** and **4** (couple IV) occur at the potentials less negative than those of compound **1**.

Fig. 8 represents the cyclic voltammogram of **5** at 0.100 V s^{-1} . Complex **5** displays a two-electron quasi-reversible reduction couple (III) at $E_{1/2} = -0.73 \text{ V}$ assigning to $\text{U}^{\text{VI}}\text{O}_2/\text{U}^{\text{V}}\text{O}_2$ and a one-electron quasi-reversible oxidation couple (I) at $E_{1/2} = 0.56 \text{ V}$ which can be assigned to the oxidation of oxime moieties since the oxidation of UO_2 center is not possible.

Acknowledgements

We thank the Research Fund of DPT (Project No: 2003K120970 and 2003K120810) and Scientific and Technical Research Council of Turkey (TUBITAK) [TBAG-AY/400 (105T002)] for financial support.

References

- [1] Melson GA. Co-ordination chemistry of macrocyclic compounds. New York: Plenum Press; 1979.
- [2] Chakravorty A. *Coord Chem Rev* 1974;13.
- [3] Sabou R, Hoelderich WF, Ramprasad D, Weinand R. *J Catal* 2005;34:232.
- [4] Preat J, Jacquemin D, Perpete EA. *Chem Phys Lett* 2005;20:415.
- [5] Yu H, Mizufune H, Uenaka K, Moritoki T, Koshima H. *Tetrahedron* 2005;61:8932.
- [6] Kachkovski OD, Tolmachev OI, Kobryn LO, Bila E, Ganushchak MI. *Dyes Pigments* 2004;63:203.
- [7] Ohta K, Moriya M, Ikejima M, Hasebe H, Fujimoto T, Yamamoto I. *Bull Chem Soc Jpn* 1993;66:3553.
- [8] Kandaz M, Yılmaz I, Keskin S, Koca A. *Polyhedron* 2002;21:825.
- [9] Kandaz M, Koca A, Özkaya AR. *Polyhedron* 2004;23:1987.
- [10] Gürol I, Ahsen V, Bekaroğlu Ö. *J Chem Soc Dalton Trans* 1992;2283.
- [11] Gümüş G, Ahsen V. *Mol Cryst Liq Cryst* 2000;348:167.
- [12] Kandaz M, Çoruhlu SZ, Yılmaz I, Koca A. *Transition Met Chem* 2002;27:877.
- [13] Ahsen V, Gürek A, Gül A, Bekaroğlu Ö. *J Chem Soc Dalton Trans* 1990;5.
- [14] Yılmaz I, Kandaz M, Özkaya AR, Koca A. *Monatsh Chem* 2002;133:609.
- [15] Kantekin H, Ocak U, Gök Y. *Z Anorg Allg Chem* 2001;627:1095.
- [16] Pavlishchuk VV, Kolotilov SV, Addison AW, Prushan MJ, Butcher RJ, Thompson LK. *Inorg Chem* 1999;38:1759.
- [17] Pavlishchuk VV, Kolotilov SV, Sinn E, Prushan MJ, Addison AW. *Inorg Chim Acta* 1998;278:217.
- [18] Panzio G, Baldrocca F. *Gazz Chim Ital* 1930;60:415.
- [19] Brintzinger H, Titman R. *Chem Ber* 1952;85:344.
- [20] Gül A, Bekaroğlu Ö. *J Chem Soc Dalton Trans* 1983;2537.
- [21] Ohta K, Higashi R, Kejima MI, Yamamoto I, Kobayashi N. *J Mater Chem* 1998;8:1979.
- [22] Bayır ZA, Bekaroğlu Ö. *Transition Met Chem* 2000;25:404.
- [23] Kurtoğlu M. *Synth React Inorg Met Org Chem* 2004;34(5):967.
- [24] Kandaz M, Özkaya AR, Cihan A. *Transition Met Chem* 2003;28:650.
- [25] Soyly S, Kandaz M, Çalışkan N. *Acta Crystallogr Sect E Struct Rep Online* 2004;60:1348.
- [26] Casellato U, Vigato PA, Vidali M. *Coord Chem Rev* 1981;36:259.
- [27] Alexander VM, Bhat RP, Samant SD. *Tetrahedron Lett* 2005;46:6957.
- [28] Kandaz M, Özkaya AR, Koca A. *Transition Met Chem* 2004;29:847.
- [29] Prushan MJ, Addison AW, Butcher RJ. *Inorg Chim Acta* 2000;300:992.
- [30] Sengottuvelan N, Manonmani J, Kandaswamy M. *Polyhedron* 2002;21:2767.